

● *Original Contribution*

## 3D RECONSTRUCTION OF CAROTID ATHEROSCLEROTIC PLAQUE: COMPARISON BETWEEN SPATIAL COMPOUND ULTRASOUND MODELS AND ANATOMICAL MODELS

BO L. LIND,\* JENS FAGERTUN,\* JENS E. WILHJELM,\* MAJA S. JENSEN,\*  
and HENRIK SILLESEN<sup>†</sup>

\*Center for Arteriosclerosis Detection with Ultrasound, Ørsted•DTU, Technical University of Denmark, Kgs. Lyngby, Denmark; and <sup>†</sup>Department of Vascular Surgery, Rigshospitalet, University of Copenhagen, Copenhagen, Denmark

(Received 17 May 2006; revised 8 January 2007; accepted 8 January 2007)

**Abstract**—This study deals with the creation of 3D models that can work as a tool for discriminating between tissue and background in the development of tissue classification methods. Ten formalin-fixed atherosclerotic carotid plaques removed by endarterectomy were scanned with 3D multi-angle spatial compound ultrasound (US) and subsequently sliced and photographed to produce a 3D anatomical data set. Outlines in the ultrasound data were found by means of active contours and combined into 10 3D ultrasound models. The plaque regions of the anatomical photographs were outlined manually and then combined into 10 3D anatomical models. The volumes of the anatomical models correlated with the volume found by a water displacement method ( $r = 0.95$ ), except for an offset. The models were compared in three ways. Visual inspection showed quite good agreement between the models. The volumes of the ultrasound models correlated with the volumes of the anatomical models ( $r = 0.93$ ), again with an offset. Finally, the overlap between the anatomical models and the ultrasound models showed, on average, that the intersection comprised 90%<sub>vol</sub> of the anatomical models and 73%<sub>vol</sub> of the ultrasound models. (E-mail: [jw@oersted.dtu.dk](mailto:jw@oersted.dtu.dk)) © 2007 World Federation for Ultrasound in Medicine & Biology.

**Key Words:** *In vitro* atherosclerotic plaque, Carotid artery, Snake, Active contours, 3D reconstruction, Volume, Tissue discrimination, Anatomical slices, Multi-angle compound imaging.

### INTRODUCTION

Advances in optimal treatment of carotid atherosclerotic plaque depend on proper identification of plaque constituents. Today, the evidence based indication for carotid endarterectomy (surgical removal of carotid atherosclerotic plaque) is based on degree of stenosis, as measured either by ultrasound Doppler methods or by contrast arteriography and, whether or not, the patient has had any symptoms of brain ischemia (MRC European Carotid Surgery Trial 1991; North American Symptomatic Carotid Endarterectomy Trial Collaborators 1991; Executive Committee for the Asymptomatic Carotid Atherosclerosis Study 1995). However, with the current knowledge of why atherosclerotic lesions induce symp-

toms and disease (Falk et al. 1995), it is evident that our way of making indications for treatment is far too simple, although the best validated available. Specifically, atherosclerotic plaque composition, *i.e.* the relative amount of constituents such as lipid, fibrous tissue and calcification and its location within the plaque, appears to be important for the prognosis (Grønholdt et al. 1998, 2001). This is difficult to access today and better imaging techniques are needed, preferably based on ultrasound. To verify possible new tissue classification methods, a reference is needed. Such a reference can be a map that shows the tissue types and their locations generated from the tissue scanned (Wilhjelm et al. 2004). However, such a comparison is not straight forward. One problem is that an ultrasound image will always be associated with a number of errors, of which some could be accepted as long as the diagnosis is unaffected. An example could be compression or expansion of an ultrasound image in the depth direction, due to variations in the speed of sound in

Address correspondence to: Jens E. Wilhjelm, Ørsted•DTU, Electronics and Signal Processing, Technical University of Denmark, Ørsted's Plads, bldg. 348, DK-2800 Kgs. Lyngby, Denmark. E-mail: [jw@oersted.dtu.dk](mailto:jw@oersted.dtu.dk)

the tissue relative to the speed of sound assumed by the scanner.

In the work of making reference maps for ultrasound images (Wilhjelm *et al.* 2004; Bridal *et al.* 1997, 1998; Hiro *et al.* 1999; Kostamaa *et al.* 1999), one of the challenges is to identify which part of the ultrasound image that should be considered as representing tissue. Here, a number of factors should be incorporated to balance between, on one side, artefacts and geometrical errors that should be identified as such, and on the other side, those that could be accepted. Another set of problems is associated with the creation of reference maps of the tissue, since the reference in itself also will be an estimate of the “true picture”.

A possible step toward the goals of identifying tissue/background in the ultrasound image and aligning this with the reference map is the creation of 3D volumetric images (reconstruction) of the plaque, where the above problems can be addressed in a consistent way. Since volume can be directly calculated, these kinds of methods are also relevant clinically, where tissue volume is an important parameter to monitor as a function of medication, dietetic treatment etc. As an example, recent studies seem to indicate that statin treatment can halt the progression of atherosclerotic plaques, as evaluated by 3D reconstruction of intravascular ultrasound imaging of coronary arteries (Nissen *et al.* 2004).

The literature clearly reveals that extraction of information from 3D ultrasound scanning of carotid plaque is challenging, both because of the dedicated data recording equipment needed and because of the pronounced artefacts in diagnostic ultrasound. Nevertheless, several *in vivo* studies have been performed on arteries and carotid plaque for the purpose of 3D visualization of the plaque and for calculation of volume (Steinke and Hennerici 1989; Delcker and Deiner 1994; Rosenfield *et al.* 1992; Ainsworth *et al.* 2005).

The application of programs for automated or semi-automated outline generation has also been studied (Steinke and Hennerici 1989; Delcker and Deiner 1994; Rosenfield *et al.* 1992; Zahalka and Fenster 2001; Mao *et al.* 2000; Gill *et al.* 1999). Some of these specify their outline generation procedure (Zahalka and Fenster 2001; Mao *et al.* 2000; Gill *et al.* 1999) and apply them with success to the lumen of the carotid artery. Other studies have investigated various sources of error in identifying plaque and measuring volume, such as inter- and intra-observer variability, effect of interslice distance etc. (Landry and Fenster 2004, 2005).

One of the problems with verification of reconstruction methods is that the ground truth is often not known. A few studies (Palombo *et al.* 1998; Landry and Fenster 2002), however, have performed measurements on precisely known phantoms and compared their volume with

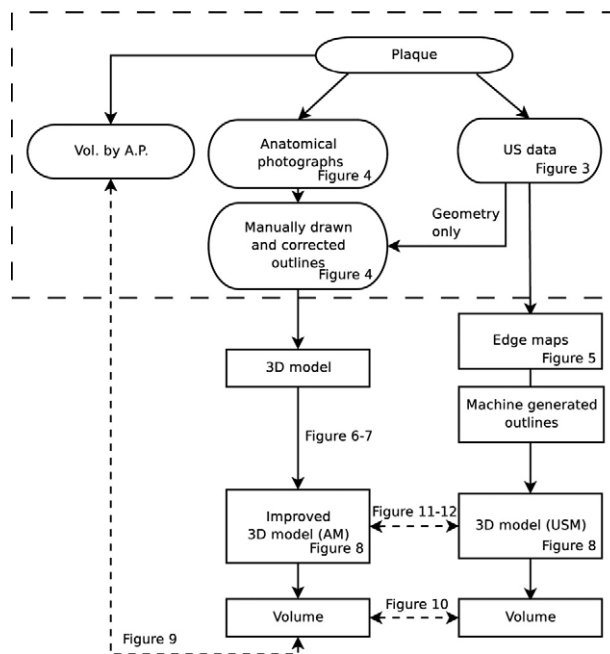


Fig. 1. The relation between the data used in this study. Rectangular boxes signify data created in this study; boxes with round corners signify data available at the start. Solid arrows indicate derived data and dashed double arrows indicate comparisons between data.

the volume estimated from 3D ultrasound reconstructions. These will be considered in the discussion.

In previous work of our group, reference maps of formalin-fixed atherosclerotic carotid plaque have been created for the purpose of automated comparisons with ultrasound-based estimates of plaque materials. A reference map has essentially the same geometrical shape as the ultrasound image and indicates the tissue type (*i.e.*, lipid rich tissue, fibrous rich tissue) in each pixel of the image. The reference map is generated from anatomical and histologic metric photographs of the tissue (Wilhjelm *et al.* 2004).

The present study used the data in (Wilhjelm *et al.* 2004) to create 3D models of the plaques for the purpose of studying how well the distinction between tissue and background can be made. Specifically, the focus is on shape, overlap and volume of 3D models derived from ultrasound images recorded with multi-angle compound imaging (MACI) and from outlines of corresponding reference maps (Wilhjelm *et al.* 2004).

## MATERIALS AND METHODS

Figure 1 shows the way in which the data used in this study is derived from one another and which comparisons are made. Each plaque (or slice of a plaque), underwent exactly the same procedure.

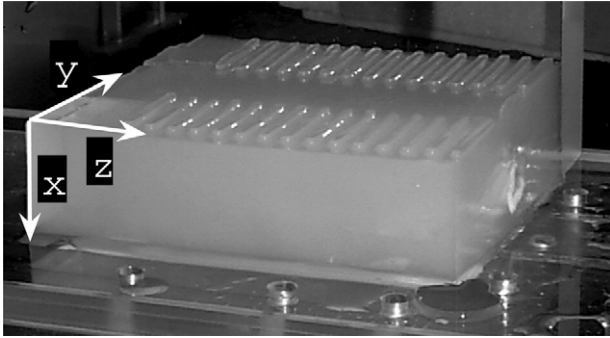


Fig. 2. Model photograph of tissue embedded in the agar block, with the axes used in this study added. The tissue shown is porcine.

#### Volume, ultrasound and anatomy data

Ten atherosclerotic plaques were obtained at carotid endarterectomy and selected randomly from a series of 119 consecutively operated patients that had experienced ipsilateral neurologic symptoms. All patients gave informed consent and the study protocol was approved by the medical ethics committee of Copenhagen and Frederiksberg counties (No. KF 01 to 375/94). The plaques were fixed in formalin after removal.

After rinsing in demineralized water, a suture was attached to the plaque and its volume was found by a water displacement technique (Archimedes' principle), using a laboratory scale (Scaltec SBC31, error below 0.001 g). The measurements were repeated the next day, and the correlation coefficient between the two volume sets were  $r \approx 0.99$  (Wilhjelm et al. 2004).

Each plaque was then placed on a support made by two sutures inside a rectangular acrylic molding frame. Liquid agar was slowly poured into the frame and, when filled, a lid with rows of rectangular openings was placed on top of the frame (Wilhjelm et al. 2004). After the agar had solidified, the lid had left a row of fiducial markers in the agar block that could both be recognized by ultrasound and later by the operator who subsequently sliced the agar block. An example of a partly sliced agar block with the markers visible can be seen in Fig. 2 and part of the intact agar block can be seen in the photograph in Fig. 8c. The fiducial markers were 1.5 mm wide and spaced 2.5 mm in the  $z$ -direction.

Pure 1%<sub>weight</sub> agar was used to optimize the contrast between tissue and background. Thus, the agar behaved much the same way as water and the assumed speed of sound of the scanner was matched to the speed of sound in water at approximately 22°C: 1485 m/s. The agar block with the plaque specimen was then placed in a scanning tank with water, and cross-sectional images interspaced 0.5 mm (in the  $z$ -direction, see Fig. 2) were recorded with the Ørsted•DTU Experimental Compound

Ultrasound Scanner (The Xtra System) (Wilhjelm et al. 2004), with an ultrasound center frequency of 7.5 MHz and a  $-3$  dB approximate width of the point spread function along the  $x$ ,  $y$  and  $z$  directions of 0.15 mm, 0.5 mm and 0.8 mm, respectively. The beams were electronically steered from a 192-element plane array transducer of length 40 mm (Wilhjelm et al. 2004).

The result of the compound ultrasound scans were between 50 and 80 images per plaque, each being  $400 \times 400$  pixel, and each pixel having 8-bit depth. An example can be seen in Fig. 3 (the outline will be explained later).

Afterwards, each agar block was cooled to 5°C (to make the agar more rigid) and then placed in a special slicing frame, in which the block could be sliced from the end, either through a fiducial marker or between two such markers (Wilhjelm et al. 2004). Slice thickness became 2.5 mm. The slicing of the agar blocks produced between 10 and 16 slices per block. Care was taken to minimize compression or deformation of the agar and plaque. Nevertheless, for some slices, the tissue deformed slightly during cutting (Wilhjelm et al. 2004). Right after cutting, but before removing the blade, the face of the 2.5 mm tissue slice was photographed (the slice was still aligned with the rest of the block). The outline of the plaque on each anatomical photograph was then traced by an operator as detailed in Wilhjelm et al. (2004). This outline was next superimposed on top of the corresponding ultrasound image and the outline was adjusted slightly where it had clearly been deformed by the

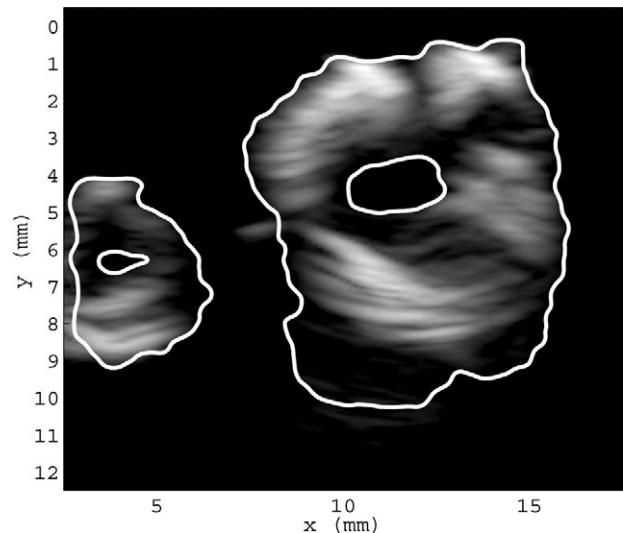


Fig. 3. The ultrasound image corresponding to the tissue seen on Fig. 4, along with the outlines found by the snake method. Note that, on the left, some of the plaque is actually outside the ultrasound image. This is observed in four of the ten plaques, with the situation shown in this picture, being the most severe. Note also that the axes in this figure and in Fig. 4 have different offsets. Dynamic range is 40 dB.

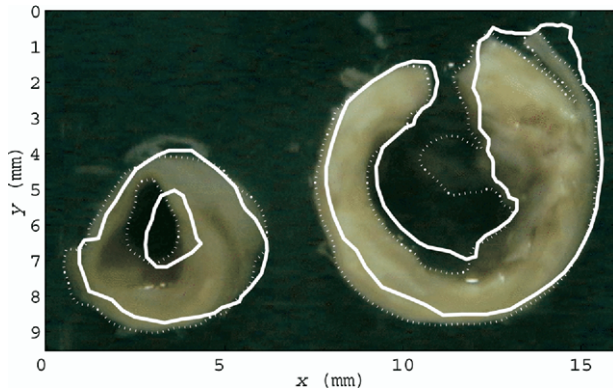


Fig. 4. The anatomical photograph along with the original (dotted) and adjusted (solid) outline.

cutting procedure (Wilhjelm *et al.* 2004). Care was taken to ensure that the area of the outline stayed constant.

An example of an anatomical photograph can be seen in Fig. 4 along with the original and adjusted outlines. It is the adjusted outline that was the basis for the reference maps in (Wilhjelm *et al.* 2004) and in the rest of the present paper; only this adjusted anatomical outline will be used.

### 2D edge detection from MACI ultrasound images

This section describes the technique used to distinguish plaque tissue from agar in the ultrasound images. This problem of medical image segmentation is difficult due to noise and speckle in ultrasound images. It has been treated widely by different applications of “active contours” (Landry and Fenster 2005), also called “snakes”, originally introduced in Kass *et al.* (1987).

The technique used in the present paper is known as a gradient vector flow (GVF) snake (Xu and Prince 1998). It can be described as a curve that moves over the image under influence from internal forces and external forces depending on the image at the current location of the snake. The sum of forces can be thought of as potential energy, much in the same way as a compressed spring.

The external energy is derived from an edge map of the ultrasound image. The edge map has high values where an edge is present and low values where there is none.

The GVF vector field is subsequently generated from the edge map. This is a vector field which points toward the edges in the edge map, while allowing for a certain (adjustable) degree of “flow” into concavities (Xu and Prince 1998). This is the basis for the calculation of the external energy of the snake at the current location.

The internal energy in the snake is given as:

$$E_{internal} = \frac{1}{2} \left[ \alpha(p) \left| \frac{\partial \mathbf{X}(p)}{\partial p} \right|^2 + \beta(p) \left| \frac{\partial^2 \mathbf{X}(p)}{\partial p^2} \right|^2 \right] \quad (1)$$

where  $\mathbf{X}(p)$  is a representation of all the coordinates in the snake with  $p \in [0, 1]$  being the time variable. The first order derivative puts a penalty on stretching and compressing, making the snake act somewhat like a spring. The second order derivative puts a penalty on bending, encouraging the snake to become as smooth as possible. The weighting parameters  $\alpha(p)$  and  $\beta(p)$  are used to control the elasticity and rigidity of the snake. This has the effect that the resulting curve is smooth, a desirable feature when segmenting plaques.

The external energy of the snake is derived from the vector field  $\mathbf{V}(x, y) = [u(x, y), v(x, y)]$  that minimizes  $E$ , with:

$$E = \int \int \mu (u_x^2 + u_y^2 + v_x^2 + v_y^2) + |\nabla f|^2 |\mathbf{V} - \nabla f|^2 dx dy \quad (2)$$

with  $\nabla f$  being the gradient of  $f$ . The first term puts a penalty on quick changes, making the field smooth, while the right hand term forces  $\mathbf{V}$  to resemble the gradient where this has a nonzero value. The external energy of the snake are the values of  $\mathbf{V}$  at the curve defined by  $\mathbf{X}$ .

At a given location of the snake in the image, both the internal and external energy can be calculated. The snake moves through the image, capturing objects of interest, by minimizing the sum of the two energies. At this equilibrium, the snake is on one hand smooth (due to the internal energy) and lies at a point of interest in the image (due to the external energy). As there are many local minima in this optimization, proper initialization of the snake is vital, as only a small subset of these minima can be classified as desirable solutions.

With this definition of snakes, the outlines in the ultrasound data set were captured. First, edge maps were generated for each ultrasound image using the Canny edge detection algorithm with parameter  $\sigma = 1$  (Canny 1986). An example of this can be seen in Fig. 5. Next, the outlines were captured with an implementation of the GVF snake. Good values for  $\alpha$  and  $\beta$  were determined through manual experimentation to be  $\alpha = 0.1$  and  $\beta = 1$ . The snake was initialized manually as a polygon that fully contained the plaque. In a few cases, such as in Fig. 4, the entire plaque was not contained in the ultrasound image, as can be seen when comparing with the anatomical photograph, seen in Fig. 5. As this only occurs in a few cases and the missing area is quite small, this is not attempted corrected. Specifically, the volume of the ultrasound model will be slightly smaller for plaques 0, 3, 9 and 10, with the slice from plaque 10 shown in Fig. 4 having the largest amount of plaque

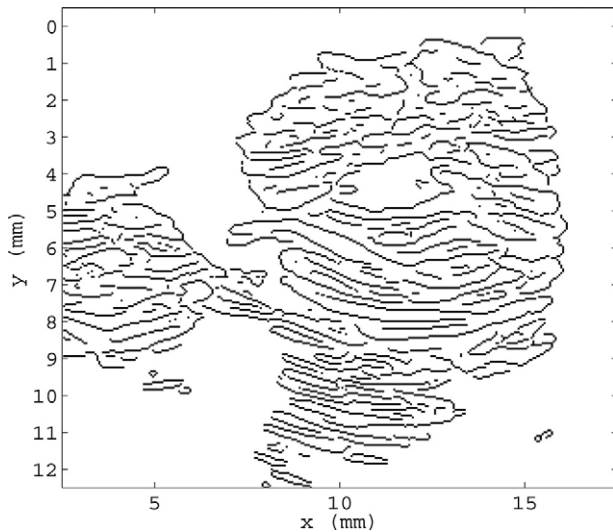


Fig. 5. The edge map (Canny et al. 1986) generated from the ultrasound image in Fig. 3.

omitted. Also, note that in a few cases, the lower part of the large outline appears unrealistically low. As seen from the bottom of Fig. 6, it is, however, captured by low gray-scale values hardly visible in the plot in Fig. 4.

### 3D reconstruction from 2D outlines

The models derived from the adjusted anatomical outlines is referred to as anatomical models (AM), while the models derived from the ultrasound images is referred to as ultrasound models (USM). When referring to both sets of models as a whole, the term 3D models will be used.

Based on the 2D outlines for both ultrasound and anatomy, the plaques were next represented as 3D models, defined by a surface. This surface, including the inner surface, consisted of triangles defined by points in space (vertices).

The outlines of every pair of adjacent scanplanes were combined to a 3D segment, which can be thought of as a “ribbon” in space, forming a cylinder-like segment. Multiple outlines in one plane were handled by either manually connecting many to one, in the case of a “Y” bifurcation or one to one, in the case of *e.g.*, an outer and an inner surface.

After all of the 3D segments were constructed, they were combined and the ends of the 3D model were closed manually. The problem of capping the ends boils down to one of triangulation of a polygon and this was done with the ear clipping algorithm (O’Rourke et al. 1998). The 3D models were finally inspected for inconsistencies to ensure that no intersecting faces were present, surfaces were closed, no double faces or vertices were present and that all faces were oriented so that their normal vectors pointed away from the tissue.

As our AMs so far have a spacing, in the  $z$  direction, which is five times that of the ultrasound data (coordinates are defined in Fig. 2), it was chosen to create additional layers of data for simpler and more fair comparison. This was done using the curved PN triangles algorithm (Vlachos et al. 2001). An illustration of this is shown in Fig. 7. More specifically, the curved PN triangles method takes a 3D model represented by faces, and, by use of the normal vectors at each vertice, generates a mathematical representation of a continuous, smooth, surface intersecting all vertices of the face-based model. Having obtained this mathematical model, the AMs were regenerated with the same spatial sampling frequency as the USMs, along the  $z$ -axis, as exemplified in Fig. 8.

### Method for calculation of volume of 3D model

Since the 3D models consisted of faces whose normal vectors were oriented away from the surface and, since the 3D models were represented by closed surfaces, the volume was calculated as the volumes of all the tetrahedra created by each single face and the origin. Volumes from faces with a normal vector pointing away from the origin were counted as positive, while volumes from faces pointing toward the origin were counted as negative. The sum of all elemental volumes yielded the volume of the 3D model. This operation was independent of the choice of origin (Gelder 1995).

### Investigation of 3D model overlap

The USM was generated from ultrasound images that were all aligned, since the transducer was translated in one direction only. Likewise for the AM. Due to the fiducial markers on the agar block containing the plaque

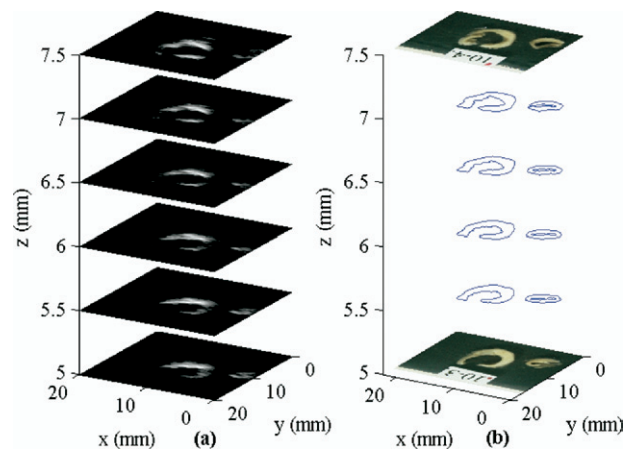


Fig. 6. (a) Six ultrasound images and (b) the corresponding two anatomical photographs. Also shown in (b) are the outlines extracted from the AM in between the two anatomical photographs. The images shown are from plaque 10, ultrasound slices 11 through 16 and anatomical slices 3 and 4.

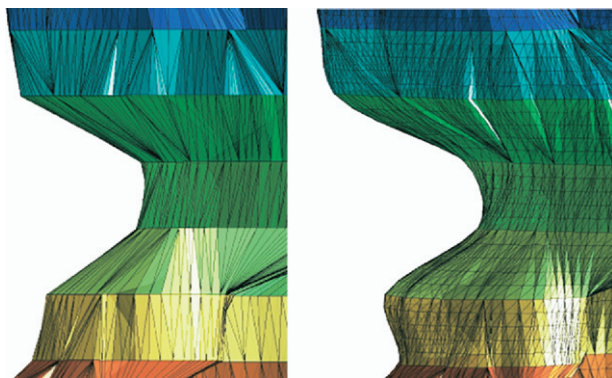


Fig. 7. Example of smoothing of 3D model by use of curved PN triangles. Untreated model on the left, smoothed model on the right.

(Wilhjelm *et al.* 2004), these two data set can also be aligned with each other. However, in the present situation, there are a number of reasons to consider the position of maximum overlap (translation only) between the two models as a slightly better method of alignment. Specifically, the motive on the ultrasound image can be slightly shifted, enlarged or deformed relative to the tissue, due to:

- Various measurement errors (mainly on the submillimeter scale) and small variations in the speed of sound in water and agar relative to the assumed speed of sound of the scanner as well as depth calibration of the experimental scanner.
- Unknown variations of the speed of sound inside the tissue.
- Artefacts (*e.g.*, by refraction) (Soetanto and Ried 1991) and the effect of the finite size of the point spread function.

In a clinical situation (Biasi *et al.* 1999; El Barghouty *et al.* 1995; Wilhjelm *et al.* 1998), the effects of these factors are unknown and not considered. Rather, the operator will, subjectively, identify the plaque tissue from the image with the errors that happens to be present. It is inside this identified region that the tissue constituents should be identified.

It is noted that for the present data set, the difference in volume overlap were up to  $\sim \lambda/2$  between using the fiducial markers for coregistering the two models and the above suggested “best alignment”.

In order to compare the AMs and the USMs in a more detailed way than the scalars representing their volumes, their intersection in space was calculated. The present 3D models were represented by faces in space. While algorithms exist to perform boolean operations on faces-based 3D models, it is much simpler to convert the 3D models to a representation by voxels and perform the

operations on these. This will yield acceptable precision provided that the number of voxels is high enough. As a compromise between computation time and precision, a voxel with side length of 0.1 mm, yielding a volume of  $0.001 \text{ mm}^3$  per voxel and an average of approx. 1.5 million voxels per plaque, was used.

Treating the voxel models as sets of voxels in space, a 3D model of the intersection between the AM and the USM ( $\text{AM} \cap \text{USM}$ ) was created, as well as the AM minus the USM ( $\text{AM} \setminus \text{USM}$ ) and the USM minus the AM ( $\text{USM} \setminus \text{AM}$ ) were calculated, for each of the 10 plaques. (The term “minus” denotes the set difference.)

## RESULTS

### 3D models

Figure 8 shows a 3D reconstruction of one of the plaques (number 10), based on the adjusted outline data and ultrasound data, along with a photograph of the plaque in agar. On the top of Fig. 3c, there is a thin “flap” of vessel wall. This is represented quite differently in the two models in Fig. 3a and b.

### Volumes and volume comparison

The correlations between the three volume measurements were investigated. The volume found by Archimedes’ principle versus AM volume can be seen in Fig. 9 while the AM volume versus the USM volume is depicted in Fig. 10.

The plot includes the perpendicular least squares regression line (dashed) and the same, only forced through the origin (dotted). It is observed that the volumes of the USMs are all larger than the volumes of the AMs, which in turn are larger than the volumes found by Archimedes’ principle.

### Overlap of 3D models

The overlapping voxels common to the AMs and the USMs were found for all 10 plaques. These sets of

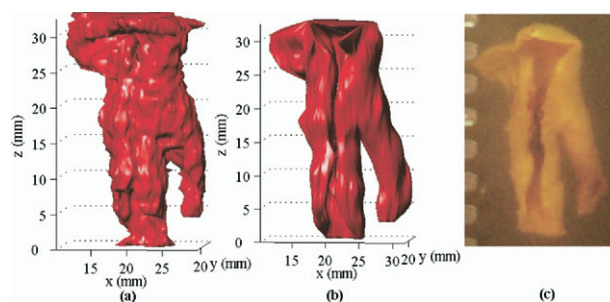


Fig. 8. 3D reconstructions of plaque 10. (a) based on adjusted outlines (AM), (b) based on ultrasound images (USM) and (c) a photograph of plaque 10 in agar (the edges of the fiducial markers are seen on the left side of the photograph). Note that the photograph is not fully aligned.

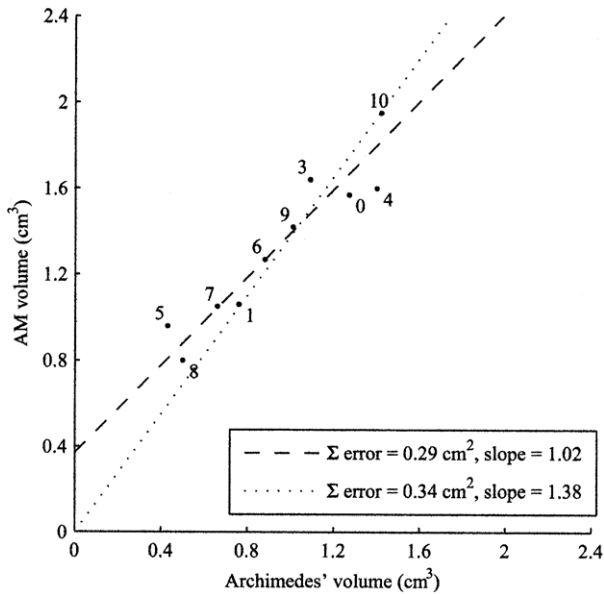


Fig. 9. Correlation between volume found by Archimedes' principle and from AMs ( $r = 0.95$ ). The dashed line is the regression line defined by the perpendicular least squares method. The dotted line is also the regression line defined by the perpendicular least squares method, but forced through the origin.

voxels were then subtracted from the 3D models. An example of all the voxels that do not overlap  $[(USM \setminus AM) \cup (AM \setminus USM)]$ , combined in one image can

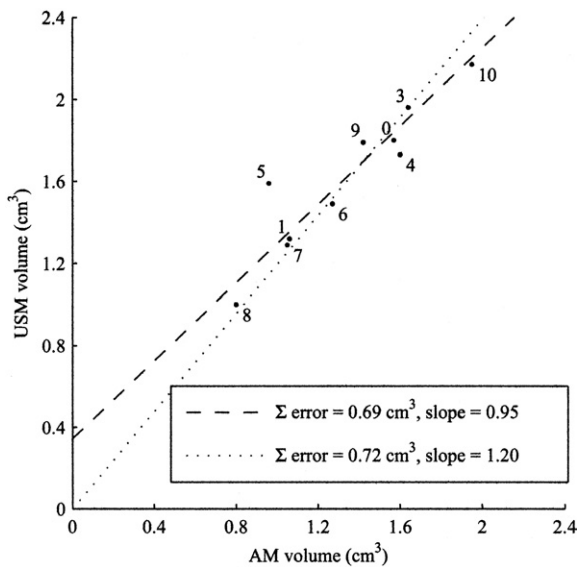


Fig. 10. Correlation between volume determined from AMs and from USMs ( $r = 0.93$ ). The dashed line is the regression line defined by the perpendicular least squares method. The dotted line is also the regression line defined by the perpendicular least squares method, but forced through the origin.

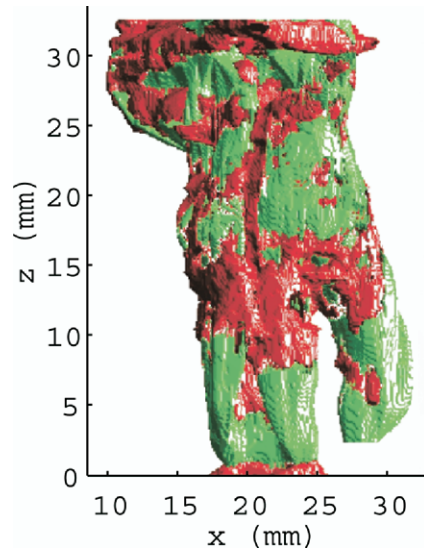


Fig. 11. The AM and the USM for plaque 10, with the intersection removed  $[(USM \setminus AM) \cup (AM \setminus USM)]$ . Red is USM only, green is AM only.

be found in Fig. 11 for plaque 10. In this particular case, there was not much difference between the volume of the AM and the volume of the USM.

The ratio between the number of overlapping voxels and the number of voxels in the AM, as well as in the USM, is shown in 12 for all 10 plaques. If the ratio is high in both bars for a given plaque, the models resemble each other well. That the black bars are consistently higher than the gray bars is a logical consequence of the volume of the USM being consistently larger than the volumes of the AM.

### DISCUSSION AND SUMMARY

The main problem of verification of the models is that there is no reference to compare against. Thus, the models can only be compared pair-wise by calculation of model overlap, by indirect methods such as volume comparisons and by subjective visual inspection. The visual inspection is discussed with respect to plaque 10, but the majority of plaques behaved the same way (data not shown).

#### Anatomical models

This study generated 10 AMs of atherosclerotic plaques based on adjusted anatomical outlines. An example of a model can be seen in Fig. 3a. Compared with photographs of the plaques, as exemplified in Fig. 3c, visual inspection shows that these AMs resemble plaque specimens quite well in general, but the surface of the AM is definitely more rough than the photograph suggests and what is realistic considering that the outer

surface of the specimen probably is representing intima and media. Likewise, the tissue flap at the upper part of Fig. 3c is not well represented in the AM. Of course, improvements of these anatomical models can be done by using a higher spatial sampling in the  $z$ -direction in future experiments. This is not an easy task, however. If the slice thickness is decreased to, say 1 mm, then the risk of tissue deformation increases. This could be counteracted by embedding the tissue in paraffin at this stage, but this in itself can cause various forms of tissue deformations. Freezing the agar block is another possibility, but if cutting is performed with a saw (Park *et al.* 2005), subsequent histologic analysis will be rendered impossible.

Another indirect indicator of model “correctness” can be found from comparison of the volume of the model with the volume measured by means of Archimedes’ principle, as shown in Fig. 9. However, neither of the two regression lines show the expected behavior of going through (0,0) and having a slope of 1. The anatomical models are consistently larger than the volume measured by Archimedes’ principle. Partial explanations for this include:

- With the low spatial sampling frequency in the  $z$ -direction, which was artificially improved as shown in Fig. 8. It is quite possible, that not all concavities were found nor that they were fully embraced by the snakes. Thus, the level of details is not as good as for the ultrasound models.
- The adjusted outlines have not been calibrated for lens distortion in the camera. (Our investigations have shown this error to be  $<1\%$ ).
- Misalignment in the camera and/or the cutting plane can have an effect on the area of the tissue on the anatomical photograph.
- Some tissue types shrink when fixed in formalin, although this depends on the methodology. A possibility is that this shrinkage might have been partially reversed when the plaques were encapsulated in agar and the formalin concentration thereby decreased.
- When the plaques were molded into the hot ( $45^{\circ}\text{C}$ ) agar, they may have swelled. This swelling may not have reversed when the agar was cooled.
- There may be tiny cracks in the surface of the plaque, which was not seen during the drawing of the outline but, nonetheless, contained water during the initial volume found by Archimedes’ principle (Wilhjelm *et al.* 2004).

The above explanations are somewhat stipulative and specific studies are needed to provide a full explanation.

### *Ultrasound models*

Visual inspection from the top of the agar block shows that these models resemble the AMs quite well; an example is shown in Fig. 3b. Many of the curvatures found on the USM can be recognized on the photograph and the tissue flap are also better represented here than in the AM. The limitations are here due to angle-dependence (Wilhjelm *et al.* 2001), the final size of the point spread function and diffraction.

Figure 10 shows a good correlation between the volumes of the 3D models, with an offset of about  $0.35\text{ cm}^3$ . If the regression line is forced through the origin, the error increases only moderately. That the USM volumes on average are  $0.35\text{ cm}^3$  bigger than the AM volumes could have various causes. First, the various parameters of the GVF snake have a large effect on the final shape and, likewise, for the starting point, defined by the user. An example of the GVF snake being too large can be seen in the lower part of Fig. 4. This could probably be tuned further to achieve better results. However, for automatic outlining of the ultrasound images, as was the original intent of this study, the number of degrees of freedom is so large that this was unrealistic to pursue further. Secondly, the ultrasound image is a distorted image of the true phantom. Typically, the motive appears bigger than the actual object scanned. This is due to several factors; they are the finite size of the point spread function, strong reflectors that create reverberations, variations in the speed of sound relative to the one assumed by the scanner as well as side lobes and grating lobes produced by the transducer. At other regions of the image, the pixel values appear very low when they actually should represent tissue. This is often due to speckle and angle-dependence.

Note that for plaques 0, 3, 9 and 10, the field-of-view of the ultrasound scanner did not cover the entire plaque in all places and the USM volumes for these plaques should in fact be slightly larger. Looking at Fig. 10, it is seen that the effect of this appears minor.

### *3D comparison*

A final way to compare the two models is in terms of model overlap. Specifically, the intersections between the AM and the USM were found by representing the models by voxels, as described previously. This discretization caused the AM volumes to become slightly larger (0.5% to 1%). The error would be smaller if the voxel size were decreased, but this would also cause the computation time to rise dramatically.

Visual inspection of Fig. 3 shows quite good agreement between the AM and the USM for plaque 10. The ratios of the intersection volume versus the AM volume

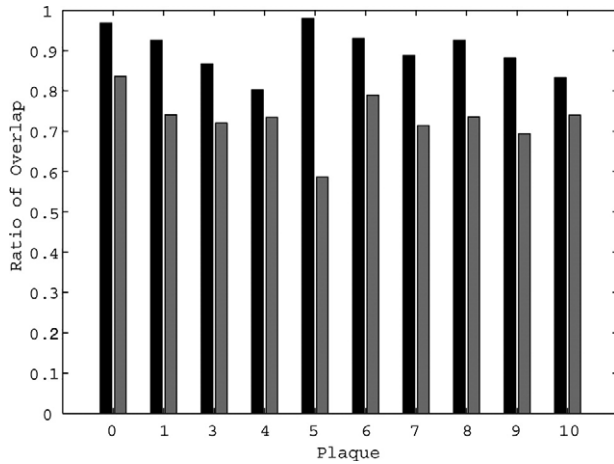


Fig. 12. For a given plaque, the AM and the USM overlap to a certain degree. This plot shows the ratio of this overlap compared with the full volume of the AM (Black, mean: 0.90) and to the full volume of the USM (Grey, mean: 0.73).

and versus the USM volume are shown in Fig. 12. It is seen that the USM makes up no less than 80% of the AM in all cases. On the other hand, ignoring plaque 5, the AM makes up 70% or more of the USM.

As stated previously, the location of the outline of the ultrasound image at high  $y$ -values seems to be the main reason for the volume of the USM being higher than that of the AM and for the overlap being lower than one. Other reasons for misfit could be: (1) the deformation of the plaques during slicing. The outlines, on which the AMs were based, were adjusted to attempt to compensate for this deformation, (Wilhjelm et al. 2004) but this might not have succeeded completely in all cases. (2) The contrast between tissue and background of some of the ultrasound images was quite poor, typically toward the two ends of the plaque, due to the relatively large extent of the point spread function in the  $z$ -direction and the effects of side and grating lobes.

In future investigations of this kind, it is suggested to trim the plaque for small tissue “flaps” before starting the study, as these (unimportant) tissue pieces present challenges to the analysis methods beyond their capabilities.

Note that at this stage, computer generated outlines are not necessarily better than manually drawn ones,

especially if this is to be done *in vivo*, where it is probably even harder to obtain precise results. However, computer generated models are promising, as some of the problems with intra- and interobserver variance inherent in manual segmentations are eliminated.

#### Comparison to literature

Only a few studies (Landry and Fenster 2002; Palombo et al. 1998), have, to our knowledge, compared the “known” volume of objects mimicking plaque with the volume estimated from corresponding 3D ultrasound images. Palombo et al. (1998) used solid bovine fibro-fatty tissue in presumably relatively regular shapes. Landry and Fenster (2002) used solid agar phantoms with scattering particles, apparently also in quite regular shapes. The present study used human atherosclerotic plaque removed by endarterectomy. Set-up and results are compared in Table 1. The right column provides the coefficient of variation between the “known” volume and the volume estimated by ultrasound. It can be seen that the more idealized the measurement situation, the higher the coefficient of variation. Especially Landry and Fenster (2002) were intended to identify the upper bound of performance and there are a number of important differences that account for the larger challenges in the present study.

Atherosclerotic plaque tissue is quite irregular, with branches and inner lumens. Thus, each scanplane can contain several inner and outer outlines. As a consequence, the ratio between plaque surface area and plaque volume is larger in the present study, giving larger room for errors in outline location and thus volume estimation.

The scattering and attenuation from (calcified) carotid plaque has a larger variation (one of the features that is attempted used for tissue classification) compared with fibro-fatty tissue and especially agar with scattering particles. Also the angle-dependence of scattering and attenuation is higher for the tissue used in the present study. This gives images with more artefacts. In general, these artefacts are more pronounced in the region below than above the plaque and, in general, our outline identification is more trustworthy at the upper part of the plaque (close to the transducer) than at the lower (*e.g.*, Fig. 4).

In the study by Landry and Fenster (2002), the volume was (apparently) found via the mass, which is a

Table 1. Comparison to literature

Study	Reference volume determined by	Tissue type	Range of actual volumes (cm <sup>3</sup> )	Outlines	$r$
Palombo et al. (1998)	Archimedes <sup>*</sup>	Regular bovine fibro-fatty tissue	0.100–0.600	Manual	0.99
Landry and Fenster (2002)	Mass	Agar with sigma cell	0.068–0.286	Manual	0.9985
This study	Archimedes <sup>*</sup>	Carotid plaque	0.430–1.420	GVF snake	0.79

very precise method. This was possible, since all samples were made from the same material. For the tissues used in (Palombo *et al.* 1998) and in the present study, Archimedes' principle had to be used, since the density could vary. Especially in the present study, direct volume measurements on wet tissue with many large and irregular surfaces are quite difficult, which could be another partial explanation for the low correlation coefficient of the present study.

## CONCLUSIONS

In this study, 10 3D models have been created based on anatomical photographs of atherosclerotic plaques and compared with 10 3D models that were generated from spatial compound ultrasound images of the same plaques.

The main aim of the paper, discriminating between tissue and background, relies on how well the models match: the models represented plaques in a convincing way, subjectively judged and judged by model overlap, even although one indicator of consistency, the volume, was consistently larger than the directly measured volume.

Several improvements are needed to increase the agreement between models. Many of the steps in the model generations were done with methods that are very application specific and sometimes very labor intensive. The anatomical 3D models generated from user-drawn outlines suffered to some degree from low spatial sampling (perpendicular to the outline plane) of the experimental procedure. The ultrasonic 3D models suffered mainly from the difficulties in generating outlines directly from the ultrasound images themselves, due to the high number of artefacts present in ultrasound image.

*Acknowledgments*—This work was supported by the Danish Technical and Medical Research Councils. The authors gratefully acknowledge the help of N. Nyssen in obtaining the density of the plaque, for which S. Nielsen, Pilot Plant, Technical University of Denmark, is also acknowledged. The authors' gratitude also extends to the anonymous reviewers for valuable comments and input.

## REFERENCES

- Ainsworth CD, Blake CC, Tamayo A, Beletsky V, Fenster A, Spence JD. 3D ultrasound measurement of change in carotid plaque volume: A tool for rapid evaluation of new therapies. *Stroke* 2005; 36(9):1904–1909.
- Biasi GM, Sampaolo A, Mingazzini P, Amicis PD, El-Barghouty N, Nicolaides AN. Computer analysis of ultrasonic plaque echolucency in identifying high risk carotid bifurcation lesions. *Eur J Vas Endovasc Surg* 1999;17(6):476–479.
- Bridal SL, Fornes P, Berger G, Lees S, Ferrair LA. Relationship between ultrasonic attenuation, apparent integrated backscatter (30 to 50 MHz) and the composition of atherosclerotic plaque. *Acoust Imaging* 1997;23:181–186.
- Bridal SL, Toussaint J-F, Raynaud J-S, Fornes P, Leroy-Willig A, Berger G. US backscatter and attenuation 30 to 50 mhz and mr t2 and 3 tesla for differentiation of atherosclerotic artery constituents *in vitro*. *IEEE Trans Ultrason Ferroelec Freq Control* 1998;45(6): 1517–1525.
- Canny J. A computational approach to edge detection. *IEEE Trans Pattern Anal Mach Intell* 1986;8(6):679–698.
- Delcker A, Diener H-C. 3D-ultrasound of the carotid arteries. *Eur J Ultrasound* 1994;1:337–344.
- El-Barghouty N, Geroulakos G, Nicolaides A, Androulakis A, Bahal V. Computer-assisted carotid plaque characterization. *Eur J Vas Endovasc Surg* 1995;9(4):389–393.
- Executive Committee for the Asymptomatic Carotid Atherosclerosis Study. Endarterectomy for asymptomatic carotid artery stenosis. *JAMA* 1995;273:1421–1428.
- Falk E, Prediman K, Shah PK, Fuster V. Coronary plaque disruption. *Circulation* 1995;92:657–671.
- Gelder AV. Efficient computation of polygon area and polyhedron. In: Paeth AW ed. *Graphics gems V AP professional*. Chap II. 1995. pp 35–41.
- Gill JD, Ladak HM, Steinmanm DA, Fenster A. Development and evaluation of a semi-automatic 3D segmentation technique of the carotid arteries from 3D ultrasound images. *Proceedings of the Conference on Medical Imaging 1999: Image Processing*, San Diego, CA. SPIE. 1999;3661:214–221.
- Grønholdt M-LM, Nordestgaard BG, Schroeder T, Vorstrup S, Sillesen H. Ultrasonic echolucent carotid plaques predict future strokes. *Circulation* 2001;104:68–73.
- Grønholdt M-LM, Nordestgaard BG, Wiebe BM, Wilhelm JE, Sillesen H. Echolucency of computerized ultrasound images of carotid atherosclerotic plaques are associated with increased levels of triglyceride-rich lipoproteins as well as increased plaque lipid content. *Circulation* 1998;97:34–40.
- Hiro T, Leung CY, Karimi H, Farvid AR, Tobis JM. Clinical investigations—imaging/diagnostic testing: Angle dependence of intravascular ultrasound imaging and its feasibility in tissue characterization of human atherosclerotic tissue. *Am Heart J* 1999;137(3): 476–481.
- Kass M, Witkin A, Terzopoulos D. Snakes—active contour models. *Int J Comp Vis* 1988;1(4):321–331.
- Kostamaa H, Donovan J, Kasaoka S, Tobis J, Fitzpatrick L. Clinical investigations—imaging/diagnostic testing. Calcified plaque crosssectional area in human arteries: Correlation between intravascular ultrasound and undecalcified histology. *Am Heart J* 1999;137(3):482–488.
- Landry A, Fenster A. Theoretical and experimental quantification of carotid plaque volume measurements made by 3D ultrasound using test phantoms. *Med Phys* 2002;29(10):2319–2327.
- Landry A, Spence JD, Fenster A. Quantification of carotid plaque volume measurements using 3D ultrasound imaging. *Ultrasound Med Biol* 2005;31(6):751–762.
- Landry A, Spence J, Fenster A. Measurement of carotid plaque volume by 3-dimensional ultrasound. *Stroke* 2004;35(4):864–869.
- Mao F, Gil J, Downey D, Fenster A. Segmentation of carotid artery in ultrasound images: Method development and evaluation technique. *Med Phys* 2000;27(8):1961–1970.
- MRC European Carotid Surgery Trial: Interim results for symptomatic patients with severe (70%–99%) or with mild (0%–29%) carotid stenosis. *European Carotid Surgery Trialists' Collaborative Group. Lancet* 1991;337:1235–1243.
- Nissen SE, Tuzcu EM, Schoenhagen P, Brown BG, Ganz P, Vogel RA, Crowe T, Howard G, Cooper CJ, Brodie B, Grines CL, DeMaria AN. Effect of intensive compared with moderate lipid-lowering therapy on progression of coronary atherosclerosis: A randomized controlled trial. *JAMA* 2004;291(9):1071–1080.
- North American Symptomatic Carotid Endarterectomy Trial Collaborators. Beneficial effect of carotid endarterectomy in symptomatic patients with high-grade carotid stenosis. *N Engl J Med* 1991; 325(7):445–453.
- O'Rourke J. *Computational geometry in C*. 2nd ed. Cambridge: Cambridge University Press, 1998.
- Palombo C, Kozakova M, Morizzo C, Andreuccetti F, Tondini A, Palchetti P, Mirra G, Parenti G, Pandian NG. Ultrafast three-dimensional ultrasound: Application to carotid artery imaging. *Stroke* 1998;29(8):1631–1637.

- Park JS, Chung MS, Hwang SB, Lee YS, Har D-H, Park H-S. Visible Korean human: Improved serially sectioned images of the entire body. *IEEE Trans Med Imaging* 2005;24(3):352–360.
- Rosenfield K, Boffetti P, Kaufman J, Weinstein R, Razvi S, Isner JM. Three-dimensional reconstruction of human carotid arteries from images obtained during noninvasive B-mode ultrasound examination. *Am J Cardiol* 1992;70(3):379–384.
- Soetanto K, Reid JM. Regions in the B-mode image of a cylinder where the location of a point reflector is changed by sound speed variation. *Ultrasound Med Biol* 1991;17(4):355–366.
- Steinke W, Hennerici M. Three-dimensional ultrasound imaging of carotid artery plaques. *J Cardivasc Tech* 1989;8(1):15–22.
- Vlachos A, Peters J, Boyd C, Mitchell JL. Curved PN Triangles. *Proceedings of the 2001 Symposium on Interactive 3D graphics*. 2001. pp. 159–166.
- Wilhjelm JE, Grønholdt M-LM, Wiebe B, Jespersen SK, Hansen LK, Sillesen H. Quantitative analysis of ultrasound B-mode images of carotid atherosclerotic plaque: Correlation with visual classification and histological examination. *IEEE Trans Med Imaging* 1998;17(6):910–922.
- Wilhjelm JE, Pedersen PC, Jacobsen SM. The influence of roughness, angle, range, and transducer type on the echo signal from planar interfaces. *IEEE Trans Ultrason Ferroelec Freq Control* 2001;48(2):511–521.
- Wilhjelm JE, Jensen MS, Gammelmark KL, Sahl B, Martinsen K, Hansen JU, Brandt T, Jespersen SK, Falk E, Fredfeldt KE, Sillesen H. A method to create reference maps for evaluation of ultrasound images of carotid atherosclerotic plaque. *Ultrasound Med Biol* 2004;30:1119–1131.
- Xu C, Prince JL. Snakes, shapes and gradient vector flow. *IEEE Trans Image Processing* 1998;7(3):359–369.
- Zahalka A, Fenster A. An automated segmentation method for three-dimensional carotid ultrasound images. *Phys Med Biol* 2001;46(4):1321–1342.